Brake Voltage Following Control of Supercapacitor-Based Energy Storage Systems in Metro Considering Train Operation State

Zhihong Yang, *Student Member, IEEE*, Zhongping Yang, *Member, IEEE*, Huan Xia, *Member, IEEE*, and Fei Lin, *Member, IEEE*

***Abstract*—The utilization of a supercapacitor energy storage system (ESS) to store regenerative braking energy in urban rail transit can achieve an energy-saving effect. This paper proposes a brake voltage following energy management strategy of ESS to adjust the charging and discharging threshold voltage based on the analysis of train operation states. The energy storage device state of charge is considered to realize the maximum usage of the ESS. First of all, the mathematical model of the dc traction power system, which encompasses the train, ESS, and traction substation, is established. Then, the energy allocation influence factors are analyzed, in particular for the double train structure. Second, under the different conditions, with the real-time monitoring of the traction network voltage and the train status, an energy management state machine is determined. Meanwhile, a set of effective state switching schemes is given to achieve the transformation of the energy management states. In the end, both the simulations using actual line data and main track field experiments prove the rationality and validity of the proposed management strategy.**

***Index Terms*—Control strategy, energy storage device (ESD), urban rail transit.**

Nomenclature

u_{ss}	Substation voltage.
u_{oc}	No-load voltage of traction power network.
u_{tm}	Traction train voltage.
u_{tb}	Braking train voltage.
u_{tma}	Traction train terminal voltage.
u_{tba}	Braking train terminal voltage.
u_{br}	Braking resistor initiated voltage.
u_{esd}	Energy storage device (ESD) voltage.
u_{ch}	ESD charging threshold voltage.
u_{cmd}	ESD charging instruction voltage.
u_{sc}	Supercapacitor (SC) voltage.
i_{ss}	Substation current.
i_{tm}	Traction train current.
i_{tb}	Braking train current.
i_{gr}	Braking train regenerative current.
i_{br}	Braking resistor current.
i_{rk}	One of the network current.
i_{cmd}	ESD charging instruction current.
i_{ch}	ESD current.
y_{ss}	Substation equivalent admittance.
y_t	Train equivalent internal admittance.
y_{ul}	Uplink line admittance at the left of a train.
y_{ur}	Uplink line admittance at the right of a train.
y_{dl}	Downlink line admittance at the left of a train.
y_{dr}	Downlink line admittance at the right of a train.
r_{ss}	Substation equivalent internal resistance.
r_t	Train equivalent internal resistance.
x_t	Distance between braking train and ESD.
ρ_n	Unit line impedance.
l_s	Distance between two adjacent substations.
p_{tm}	Traction train power.
p_{tb}	Braking train power.
p_{esd}	ESD power.
p_{ss}	Traction substation power.
p_{br}	Braking resistor absorbing power.
E_{sc_dis}	SC-ESD discharging energy.
E_{sc_ch}	SC-ESD charging energy.
E_{sub}	Traction substation supplied energy.
E_{tra}	Total traction energy.
η	Energy conservation rate.

Manuscript received March 31, 2017; revised September 2, 2017 and November 19, 2017; accepted December 19, 2017. Date of publication January 15, 2018; date of current version April 2, 2018. This work was supported in part by the National Key Research and Development Program of China under Grant 2017YFB1201105-05 (2017–2020) and in part by The Research and Development Plan of the Ministry of Science and Technology under Grant 2016YFB1200506-18 (2016–2020). *(Corresponding author: Zhihong Yang.)*

Z. Yang, Z. Yang, and F. Lin are with the School of Electrical Engineering, Beijing Jiaotong University, Beijing 100044, China (e-mail: 15121496@bjtu.edu.cn; zhpyang@bjtu.edu.cn; flin@bjtu.edu.cn).

H. Xia is with the Beijing Institute of Space Launch Technology, Beijing 100076, China (e-mail: huanhuan7000@gmail.com).

Color versions of one or more of the figures in this paper are available online at http://ieeexplore.ieee.org.

Digital Object Identifier 10.1109/TIE.2018.2793184

I. Introduction

With the continuous development of society in China, the Chinese urban rail transit system has expanded rapidly. However, this system consumes a tremendous amount of energy. Therefore, it is of practical significance to research energy conservation. Considerable amounts of energy can be saved in the urban rail transit system with the application of a supercapacitor (SC) energy storage system (ESS) [1].

Due to the fact that on-board storage increases the weight and space of a vehicle, ground storage is widely used. SC, as an emerging energy storage element with a high power density, a long cycle life period, and a wide temperature range, has become the most suitable storage component paired with the operation characteristics of an urban rail transit [2]–[4].

For the control aspect of ESS converters, a bidirectional dc/dc converter is used to control the energy flow [5]–[8]. In order to realize rapid and stable control, the double loop control strategy of the voltage outer loop and current inner loop with PI regulators is widely used in the control of energy storage converters, due to its ease of parameter tuning [9]–[12].

The charging and discharging control strategies, which are based on a traction network voltage control ESD, are widely applied [12], [13]. The main concept involves how to set the appropriate threshold [14], [15]. Based on a variety of optimization goals, several improved energy management strategies have been previously proposed. One of them is a strategy that considers the minimum energy consumption, in which the functions of ESD and train operation curve were established, and the strategy was optimized by the sequential quadratic programming [16]. In many studies, the traction network voltage is considered to be the controlled object, while the energy consumption is reduced with the decrease in the dc line loss by reducing the RMS value of the output current of the ESS [17], [18]. While considering the continuous distribution impedance of the traction power supply network, the network voltage in different train positions was analyzed [19], [20]. In order to precisely control the SC state of charge (SOC), a three-loop control strategy, based on the typical double loop control strategy, was improved, in which the feasibility of the voltage loop was nested in the traction network voltage loop, and the SC current loop was analyzed to realize accurate control of the SC-ESS voltage and SOC [13], [21].

However, at present some deficiencies remain in the research regarding the energy management strategy of the ground SC-ESS. It is necessary to consider the regenerative braking energy transferred between trains and to further distribute the remaining energy between the ESD and train brake resistor. In order to successfully perform the energy flow analysis among traction substations, trains, and ESDs, as well as to achieve the maximum usage of regenerative braking energy, this paper proposes a control strategy for ESDs, based on the consideration of train operation states.

This work is organized as follows: In Section II, a mathematical model of the traction power supply system considering ESS is established, which, based on the double train operation structure, is used to analyze the energy distribution. In Section III, a brake voltage following energy management strategy considering the train operation state is proposed. In Section IV, a simulation with the actual data of the Beijing Batong Subway Line is used to validate the control strategy. In Section V, the results of main track field experiments are shown. Finally in Section VI, a summary is given.

II. Power Flow of ESS

A. Traction Power Supply System Equivalent Model

The dc power supply network of an urban rail transit and its energy flow are shown in Fig. 1 [1], [22]. The ESS is installed

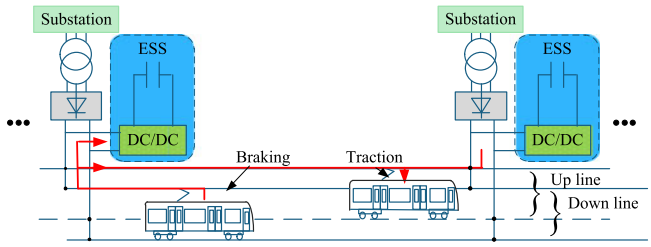

Fig. 1. Structural diagram of a dc traction power system.

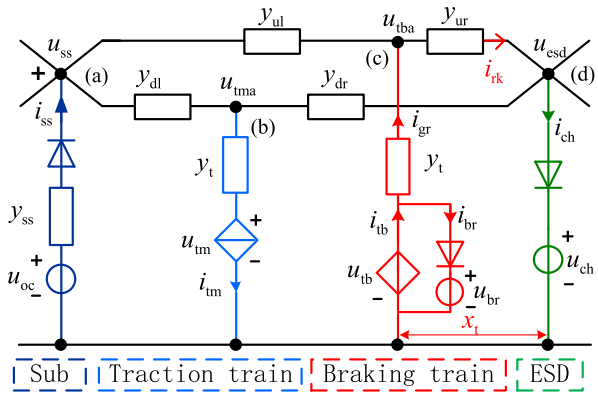

Fig. 2. System structure diagram of a double-train operation.

in the traction substation, paralleling the dc bus [23], [24]. The traction train would gain the powering energy from substations, regenerative braking energy of the near trains, and the ESS. The regenerative braking energy can be restored in the ESS and can be used for the next energy requirement.

In order to analyze the power distribution in the traction network, an equivalent model is established including the traction and braking trains, as shown in Fig. 2, in which the application of an ESD is considered. When the line loss is slightly compared with the train operation power, the substations and ESDs on both sides can be equivalent to 1 for the entire traction power supply network. In this paper, the equivalent model assumes that there is one substation on the left side, one ESD on the right side, and the traction train and braking train are located between the two. The substation is described as the Thevenin equivalent model and is represented by an equivalent internal resistance and an ideal voltage source in series. The braking train contains the brake resistor paralleled with the equivalent power source of the train [25]–[27].

In the model, the traction substation, ESD, and braking resistor are connected in series with a diode, respectively, and each diode has two states, i.e., shutting off and conducting, represented as "0" and "1", respectively; thus, the topology of the model includes eight states, from "0" to "7", with binary encoding. In graphics, the lowest common node can be considered as a reference node, and then the circuits, respectively, between the (a)–(d), nodes and the reference node can be seen as an independent branch.

For the system, the braking train branch is considered as a whole, while the braking resistor is an internal part. Therefore, first the node voltage equations of the equivalent operation system are set up as (1)–(4), respectively,

TABLE I
EIGHT STATES OF DOUBLE TRAINS OPERATION MODEL

States	Substation	ESD	Brake resistor	Node voltage equations
0	0	0	0	–
1	0	0	1	(5), (2), (3), (6)
2	0	1	0	(5), (2), (3), (4)
3	0	1	1	(5), (2), (3), (4)
4	1	0	0	(1), (2), (3), (6)
5	1	0	1	(1), (2), (3), (6)
6	1	1	0	(1), (2), (3), (4)
7	1	1	1	(1), (2), (3), (4)
Branch current equations	(9)	(10)	(11)	–

shown below, corresponding to each branch with nodes (a)–(d):

$$\begin{cases} u_{ss}(y_{ss}+y_{dl}+y_{ul})-u_{tma}y_{dl}-u_{tba}y_{ul}-u_{oc}y_{ss}=0 & (1)\\ u_{tma}(y_t+y_{dl}+y_{dr})-u_{ss}y_{dl}-u_{esd}y_{dr}-u_{tm}y_t=0 & (2)\\ u_{tba}(y_{ul}+y_{ur}+y_t)-u_{ss}y_{ul}-u_{esd}y_{ur}-u_{tb}y_t=0 & (3)\\ u_{esd}(y_{ur}+y_{dr})-u_{tba}y_{ur}-u_{tma}y_{dr}+i_{ch}=0. & (4) \end{cases}$$

With the three diodes considered, the voltage equations of nodes (a) and (d) are diverse with different diode states. Thus, with $i_{ss}=(u_{oc}-u_{ss})y_{ss}=0$ shown in (5), and with $i_{ch}=0$, which is set as follows:

$$u_{ss}(y_{dl}+y_{ul})-u_{tma}y_{dl}-u_{tba}y_{ul}=0 \quad (5)$$

$$u_{esd}(y_{ur}+y_{dr})-u_{tba}y_{ur}-u_{tma}y_{dr}=0. \quad (6)$$

Therefore, (1), (4), (5), and (6), respectively, display conditions with $i_{ss}\neq 0$, $i_{ch}\neq 0$, $i_{ss}=0$, and $i_{ch}=0$.

Second, the current inside the branches will be further analyzed. The train power and current expressions are shown, respectively, in the following equations:

$$\begin{cases} p_{tm}=u_{tm}i_{tm}\\ p_{tb}=u_{tb}i_{tb} \end{cases} \quad (7)$$

$$\begin{cases} i_{tb}=i_{gr}+i_{br}\\ i_{tm}=(u_{tma}-u_{tm})y_t\\ i_{gr}=(u_{tb}-u_{tba})y_t. \end{cases} \quad (8)$$

The different conditions of diode conduction and turn-off, in which the rectifier units, ESD, and brake resistor, respectively, meet constraints are shown as follows:

$$i_{ss}=(u_{oc}-u_{ss})y_{ss} \quad (9)$$

$$i_{ch}=(u_{tba}-u_{ch})y_{ur}+(u_{tma}-u_{ch})y_{dr} \quad (10)$$

$$i_{br}=i_{tb}-(u_{tb}-u_{tba})y_t. \quad (11)$$

With the binary coding, Table I shows the eight states corresponding to Fig. 2, and it also shows the branch current and node voltage constraint equations corresponding to each state. The code "1" means that the device on this branch is in the conduction state, satisfying the branch current equation separately as shown in (9)–(11), respectively, and corresponds to the substation, ESD, and brake resistor in an operative mode. Accordingly, the "0" code means that the device on this branch is OFF, and the current of this branch does not need to be calculated.

Under the observation of eight states, the braking resistor operates to consume the brake energy in states 1, 3, 5, and 7, which is not energy efficient, and should be avoided. States 2 and 4 are reasonable states, where the tractor power p_{tm} is less or greater than the braking power p_{tb}, and the remaining braking power is absorbed by the ESD or excess part is supplied by the substation. State 6 is similar to state 5, where the remaining regenerative energy is restored in the ESD, while there is different energy saving effects.

Take state 1 as an example, only the resistor is valid with $i_{ss}=0$ as shown in (5), and $i_{ch}=0$ as shown in (6). The node voltage equations of nodes (b) and (c) are immobile as shown in (2) and (3). Meanwhile, the branch with resistor meet the current (11). Therefore, the voltage and current of different branches would be obtained.

The brake resistor, station, and ESD are placed in and correspond to varied power statuses of the different branches which the components are located in. Similarly, we can determine the analytical equations of the traction network in different states, by combining node voltage equations with different boundary conditions in various states, as displayed in Table I. Then, the energy flow in different system states can be analyzed.

B. Position Effect on Energy Distribution

According to the equations analyzed above in Section II-A, the relationship between p_{tb} varying from 0 to 2 MW and p_{tm} changing from 0 to 4 MW can be solved. The brake resistor initiated voltage u_{br} is 920 V assuming that the charging threshold voltages u_{ch} are fixed as 872, 908 and 920 V, respectively, which are in the range between the no-load voltage 860 V and the braking resistor initial voltage 920 V. When the braking train is close to the ESD, x_t, shown in Fig. 2, is 0.1 km, and the results are shown in Fig. 3(a)–(c), while in Fig. 3(d), (e), and (f), $x_t=$ 1.9 km, and the states are shown in Fig. 3.

From Fig. 3, when the braking train is close to the ESD, under the condition that u_{ch} is 872 V, i.e. close to the u_{oc}, then the working states are only 2, 4, and 6. Too low voltage of ESD affects the power transmission between two trains. When the u_{ch} is 908 V, i.e., close to the u_{br}, the working states of 1, 3, and 5 appear, and the brake resistor is activated, as the high level of charging voltage would boost the braking train voltage. When u_{ch} rises up to 920 V, the working states of the system are 1, 4, and 5, in which the high u_{ch} will result in the initiation of the braking resistor consuming energy.

In order to make use of regenerative braking energy as much as possible, the energy interaction between multiple trains should be improved. The state of "6" with substation supplies energy to ESD needed to be avoided. Thus, a low charging threshold voltage of ESD can absorb the most interaction energy between trains. The threshold should be adjusted higher, but also avoid the starting of braking resistor.

In the condition when the braking train is located far away from the ESD, comparing with the short distance condition, state 3 appears instead of state 6. Thus, the rectifier unit does

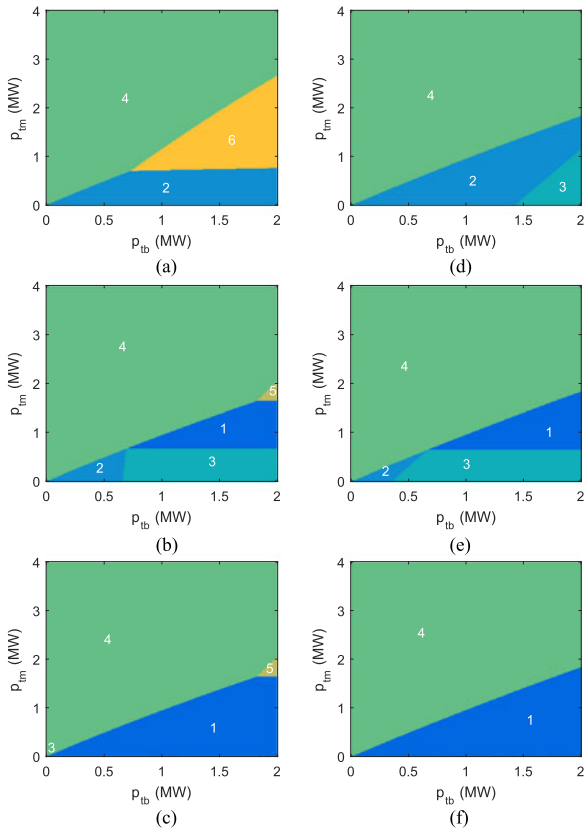

Fig. 3. Power distribution with different positions. (a) u_{ch} = 872 V, (b) u_{ch} = 908 V, (c) u_{ch} = 920 V, (d) u_{ch} = 872 V, (e) u_{ch} = 908 V, and (f) u_{ch} = 920 V.

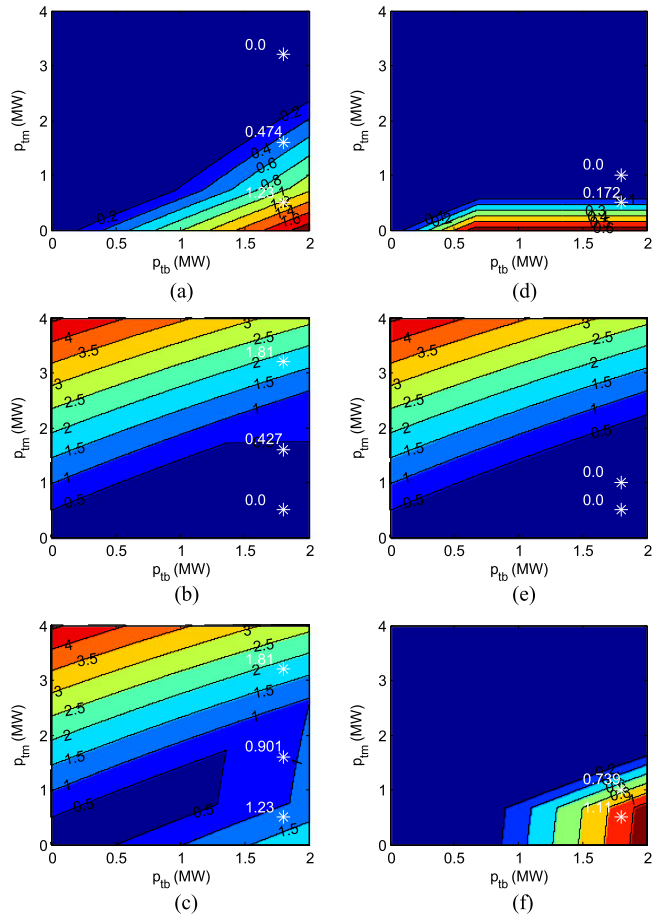

Fig. 4. Power distribution with different charging threshold. (a) P_{esd}(MW), (b) P_{ss}(MW), (c) P_{csm}(MW), (d) P_{esd}(MW), (e) P_{ss}(MW), and (f) P_{tb}(MW).

not provide power to the ESD. However, it is not energy conservation but energy consumption in the brake resistor. On the high u_{ch} condition, even in the case of high braking energy, the major area is occupied by state 4, and the regenerative braking energy is not fully utilized. Just like the short distance condition, the u_{ch} is too high to store the charged energy into the ESD.

Therefore, the short distance between braking train and the ESD would be satisfied for the ESD to realize the usage of remaining regenerative braking energy. In the next section, the effluence of charging threshold would be further studied.

C. Charging Threshold Voltage Effect on Energy Distribution

Based on the analysis in Section II-B, taking the braking train close to the ESD as the model, $x_t = 0.1$ km and u_{ch} with 872 and 908 V are taken into account.

Fig. 4(a)–(c) falls under u_{ch} = 872 V, and p_{csm} is the power sum of ESD and substation; the conditions under the threshold of u_{ch} = 908 V are shown in Fig. 4(d)–(f). Each line in the graph is a power contour line. The p_{tb} = 1.8 MW is taken as an example and as an axis. Looking from the bottom, the corresponding power of the substation, ESD, and brake resistor can be obtained at the different p_{tm} power levels. The values of which are marked with tab "$*$" in the graphs.

When the u_{ch} is as low as 872 V, as shown in Fig. 3, the working states are 2, 4, and 6. Then, the 0.5, 1.6, and 3.2 MW of traction power are selected separately in the three states.

When the p_{tm} = 0.5 MW, the traction power is very small, and the ESD voltage will be stable at 872 V, after which all the traction power 0.5 MW is derived from the braking train. The remaining energy 1.23 MW is charged into ESD. This is the typical state of the system under state 2. With the increase in the traction power, when p_{tm} raises up to 1.6 MW, the u_{esd} remains at 872 V. However, when the system is in state 6, the substation should provide power to the traction train. In fact, only a part of the traction power is supplied by the braking train, while the others are derived from the substation, and remaining regenerative braking power is absorbed by the ESD. Thus, there is an unexpected circulation between the substation and ESD. The reason for this phenomenon is that the traction power is relatively large, and the terminal voltage of the traction train is pulled down, which make the substation to start its operation. When the traction power continues to rise up to 3.2 MW, the braking energy is insufficient to provide energy, and the substation supplies the energy in state 4.

When the u_{ch} is higher, reaching 908 V, the high voltage initiates the operation of the brake resistor to consume energy. Same as low charge voltage situation, the substation supplies

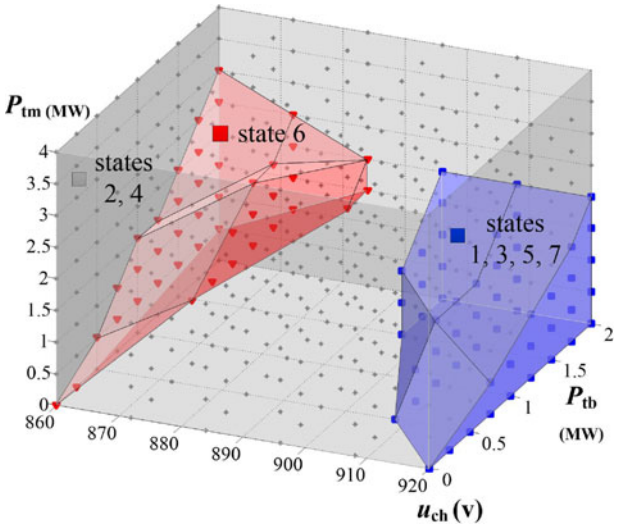

Fig. 5. State range dot matrix with three regions.

power with the large traction power. Assuming that the traction power is 0.5 MW in state 3 and 1 MW in state 1, in addition to charging the ESD, the remaining regenerative braking energy will be consumed by the braking resistor.

By the horizontal contrasting, under the high charging voltage, even with the small value of traction power, the brake resistor consumed energy.

Therefore, the operation states of the double train system are not only related to the traction and braking power of the two trains, but also to the charging threshold voltage u_{ch} of the ESD. Based on the above analysis, the state range dot matrix of the three variables is plotted as a cube as shown in Fig. 5. The substation no-load voltage is 860 V and the braking resistor initial voltage is 920 V. The diagram is composed of many coordinate dots. The charging threshold voltage, traction power, and braking power make up a cube space of dot matrix.

Only at certain traction or braking power, and when the u_{ch} varies in a proper value, the system can work in the appropriate states 2 or 4. Actually, in transformation, there are different states at any time in variety power and threshold voltage. In state 1, 3, 5, and 7, the brake resistor is activated. The control strategy proposed in this paper hopes to make the system work in the state 2 or 4 as much as possible. Thus, the whole cube is divided into three parts.

In summary, the impact of u_{ch} on the traction power supply system is as follows:

1) u_{ch} affects the power transferred from the brake to the tractor when u_{ch} is low, thereby causing the braking power to be absorbed by the ESD. From another perspective, the extra power absorbed by the ESD is derived from the substation, which is equivalent to the formation of the circulation between the rectifier unit and ESDs, and will increase the workload of the SC-ESD with a limited capacity.
2) u_{ch} and p_{tb} are excessively high, and thus, the u_{ch} affects the charging power of the ESD, and part or even all of the remaining energy which should be filled by the ESD is consumed by the braking resistor. This weakens the energy saving effect, and results in waste of energy.
3) The appropriate u_{ch} will allow the system to operate in a state in which the rectifier or ESD works alone. However, the optimal u_{ch} is not fixed, and will vary with the network and train states. In order to guarantee the system operation in an optimal state, it is necessary to design the u_{ch} based on the train status, so as to allow the system to operate in the best state in real time.

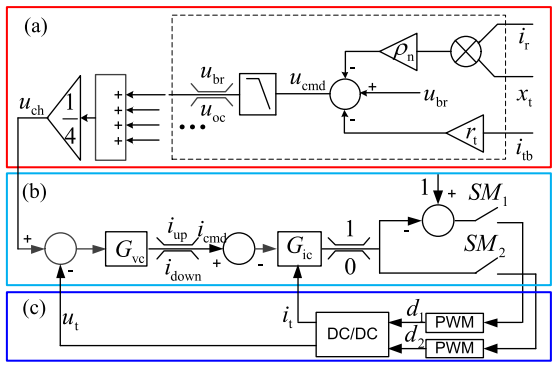

Fig. 6. Brake voltage following charging control strategy. (a) Brake voltage following charging control strategy module, (b) double closed-loop control of ESS module, and (c) hardware in loop control module.

III. Proposed Control Strategy

A. Brake Voltage Following Control Strategy

Based on the previous sections of the train operation states analysis, the ESD charge threshold voltage u_{ch} should be dynamically adjusted according to the train operation states in order to allow the traction power supply system to work in the most energy saving manner in states 2 or 4.

u_{ch} should be adjusted to make the brake train voltage u_{tb} slightly smaller and close to the brake resistor initiated voltage u_{br}, so that the train braking resistor is not activated. Fig. 2 also shows a schematic diagram of the system with the braking train. The x_t is the distance between the braking train and the ESD, and i_{rk} is its corresponding current. This is one of the four currents connected to the ESD, while the control of the ESD is $u_{cmd}(k)$, as the instruction voltage shows in (12), shown below, and i_{tb} can be measured by the current sensor on the traction substation feeder. x_t can be obtained from the train control signal

$$u_{cmd}(k) = u_{br} - (i_{tb}(k)r_t + i_{rk}x_t(k)\rho_n)\,. \tag{12}$$

The control block diagram of the ESD based on the train states is shown in Fig. 6. The control block can be divided into three parts, which, from top to bottom, are the proposed brake voltage following control strategy module, double closed-loop, and hardware in loop control module.

In the proposed brake voltage following the charging control strategy module, the part in the dashed frame exactly matches (12), and u_{cmd} must be filtered by a low-pass filter to avoid the influence of the converter control loop. The filter can be a first-order low-pass filter, among them, and the τ_{lpu} is a time constant. Meanwhile, the optimal charging voltage with the mean value of

four control voltages corresponding to the braking trains, which exist on the four branches connecting to the ESD, is calculated by the following:

$$u_{\mathrm{ch}} = \frac{1}{4}\sum_{\mathrm{k}=1}^{4}\left[\frac{1}{\tau_{\mathrm{pu}}s+1}u_{\mathrm{cmd}}(k)\right]. \tag{13}$$

Aiming at the energy management research of the ESD, the classical energy management strategy is the double loop control strategy. Based on it, the proposed braking voltage following method is combined to realize the energy management considering the train operation conditions. The double loop control strategy realizes the voltage outer loop and current inner loop control, and both internal and external loops adopt the PI regulator. G_{vc} is the regulator of the voltage outer loop. Through the current amplitude limiting with the upper and lower value of i_{up} and i_{down}, the ESD command current i_{cmd} is obtained. G_{ic} is an internal current regulator with the same amplitude limiting range of 0–1.

In the hardware-in-loop control module, $SM1$ and $SM2$ are the pulse select switches, respectively, and obtain the duty cycle signal from internal current regulator. Then, PWM1 and PWM2 generate control pulses to, respectively, turn ON and OFF the upper and lower arm IGBT of the dc/dc converter.

In order to verify the proposed control strategy, (12) is substituted into the equations of the eight states in the Section II. The influences of train location and ESD threshold voltage on the system energy distribution are analyzed. Thus, the proposed control strategy is used to simulate the states at different locations. The states, respectively, corresponding to the x_{t} of 0.1, 0.46, 0.82, 1.18, 1.54, and 1.9 km conditions are counted. In the former three positions, the states are 2, 4, and 6. However, in the latter three positions, states are 2 and 4.

It can be clearly seen that most states of the system are states 2 and 4. In the data statistic process, only when the train is close to the ESD, and in the vicinity of $(p_{\mathrm{tm}}, p_{\mathrm{tb}}) \approx (1.75, 1.85)$ MW will there be a small area of state 6. In others, the brake resistors are no longer activated. Therefore, the system can always be in the best state after using the brake voltage following strategy.

Taking one of them as an example for further analysis. When $x_{\mathrm{t}} = 0.46$ km, the voltage and power contours are shown in Fig. 7. In Fig. 7(a), the u_{tb} can always be maintained under or at u_{br}, and the energy can be transmitted to the traction train. In Fig. 7(b), the u_{esd} is higher when the p_{tb} and p_{tm} are very small, and gradually reduced to u_{oc} with the increase in p_{tb} and p_{tm}. From Fig. 7(c) and (d), which are fixed with a vertical axis, the p_{esd} is first gradually decreased to 0, and then, the p_{ss} rises with the increase in the p_{tm} because the high traction power pulls down the traction train terminal voltage.

B. Energy Management Policy State Machine

In the ESD working process, in addition to monitoring the traction network voltage and train states in real time, it is necessary to give an effective set of state switching schemes. Therefore, the flow chart of energy management state machine is given, as shown in Fig. 8, where $u_{\mathrm{sc,low}}$ and $u_{\mathrm{sc,high}}$ directly reflect the lowest and highest SOC of the SC.

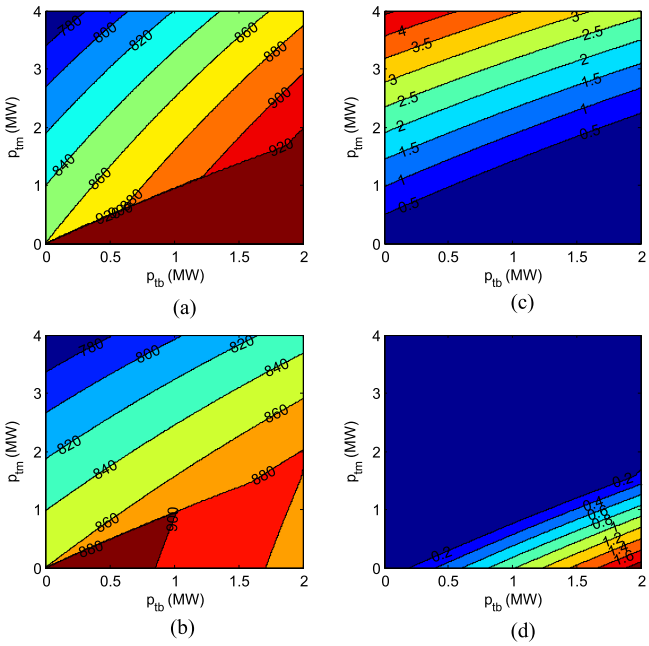

Fig. 7. Power distribution in $x_{\mathrm{t}} = 0.46$ km. (a) U_{tb} (V), (b) U_{esd} (V), (c) P_{ss} (MW), and (d) P_{esd} (MW).

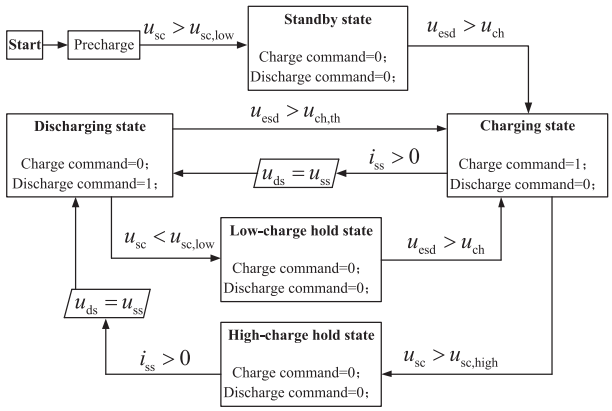

Fig. 8. Flow chart of energy management state machine.

As the system is initiated, it goes into the standby mode when charging and discharging are not allowed. Due to the low voltage of the SC, the system waits for the train to brake, and the ESD is charged. The condition of jumping out of the standby is as follows: ESD voltage is larger than the ESD charge instruction voltage, i.e., $u_{\mathrm{esd}} > u_{\mathrm{ch}}$. After jumping out of the standby mode, the system operates in the charging state. The charging instruction is set to "1." There are two conditions when out of charging, the first being when substation current $i_{\mathrm{ss}} > 0$ and, then, the system directly jumps to the discharging state. In the beginning of the discharging process, it is an assignment of the discharging threshold voltage that makes u_{ds} equal to u_{ss}. The discharging voltage is approximately same as the substation no-load voltage can realize the maximum discharge power of ESS. The second is when the SC voltage is higher than the maximum voltage value of SC, i.e., $u_{\mathrm{sc}} > u_{\mathrm{sc,high}}$, that is, the

TABLE II
PARAMETERS OF POWER SUPPLY SYSTEM

Parameters	Value	Parameters	Value
u_{oc}	860 V	ρ_n	0.016 Ω/km
l_s	2 km	u_{br}	920 V
r_t	0.015 Ω	r_{ss}	0.0161 Ω

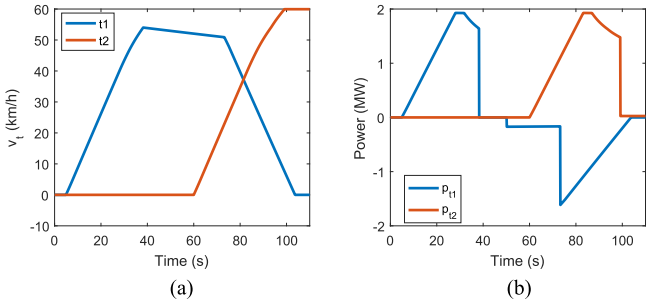

Fig. 9. Trains velocity and power curve of traction and brake conditions staggered.

SC has reached its maximum storage capacity, and the system enters the hold state.

In the discharging state, the charging instruction is "0" and the discharge instruction is set to "1." The discharge state is similar to the charge state, namely there are two jump conditions. Actually, the whole research contains a complete set of charging and discharging conversion process, however, due to space limitation, this paper focuses on the introduction of the charging process control strategy.

In the two hold states, the instructions of both are "0" and only have one jump out condition. The advantage of using this energy management strategy is preventing the system from generating state oscillations in the case of filling or emptying.

IV. SIMULATION VERIFICATION

The present paper builds a traction supply system model in MATLAB/Simulink to verify the proposed braking voltage following control strategy. The SC capacity is configured as 294 F with the rated voltage of 750 V, based on the Beijing Subway Batong Line parameters of the traction power supply system for quantitative analysis, as shown in Table II.

Now, two extreme states are used to validate the proposed strategy. One is in a low charging threshold voltage, it is likely that substation will supply power to ESD; another is in a high charging threshold voltage and brake resistor is easy to be activated. Fig. 9 displays the velocity and power curve of online trains. In this part, subscript "t1" means the first train, and "t2" is the second train.

In the first condition, the No. 2 train begins to undergo traction and move away from the ESD, while the No. 1 train brakes closely to it. When $u_{ch} = 865$ V, the overlapping of traction and brake conditions are shown in Fig. 10(a). In the charging process, the u_{esd} remains at 865 V, and at 73.3 s, the u_{t1} reaches a maximum voltage of 896 V. In Fig. 10(b), the ESD and substation both discharge with a large traction power. However, in the

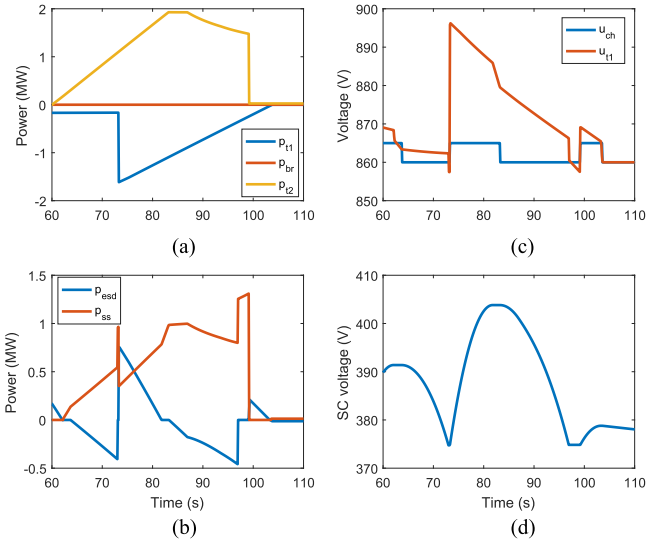

Fig. 10. Simulation results when $u_{ch} = 865$ V.

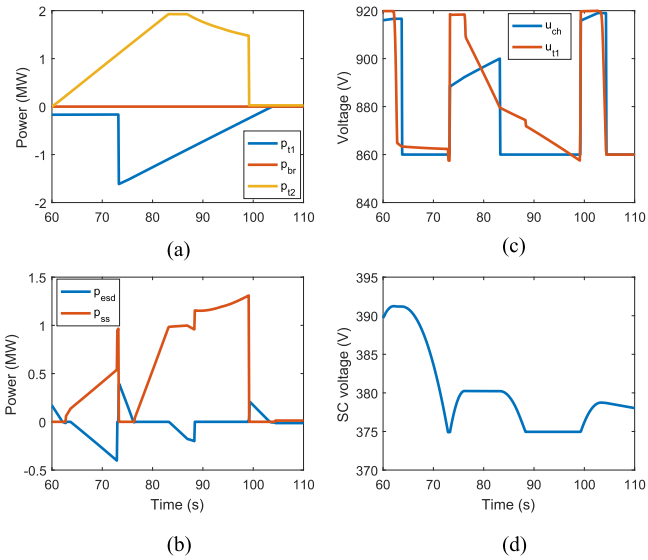

Fig. 11. Simulation results of brake voltage following control with short distance.

period of 73.4–82 s, a state of $p_{esd} > 0$, $p_{ss} > 0$ sustains. This is not expected that the virtual energy circulation between the substation and ESD occurs. During this time, the u_{sc} is charged from 375 to 404 V.

Under the proposed control strategy, the results with the same train conditions are shown in Fig. 11. In Fig. 10(c), u_{ch} is dynamically adjusted, allowing u_{t1} to rise up and maintain a close distance to u_{br}. In Fig. 10(b), it is shown that the ESD charges while the rectifier unit is in the powering state. In Fig. 10(d), u_{sc} changes from 375 to 380 V during 73.4–82 s. There is no undesired circulation between ESD and substation generated.

In another case, the brake train is far away from the ESD, the velocity and power curve of two trains are also shown as Fig. 9, but the No. 2 train is delayed, as shown in Fig. 12(a). Under the fixed charge threshold voltage, Fig. 12(a)–(d) shows the operation result when $u_{ch} = 910$ V. In Fig. 12(a), due to the

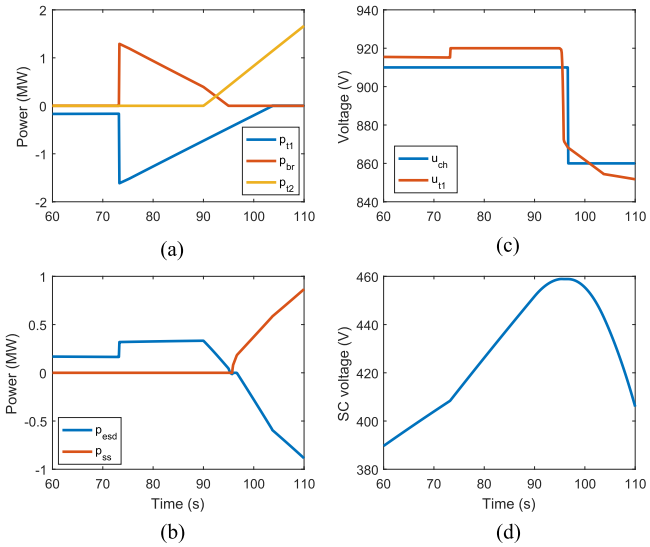

Fig. 12. Simulation results when $u_{ch} = 910$ V.

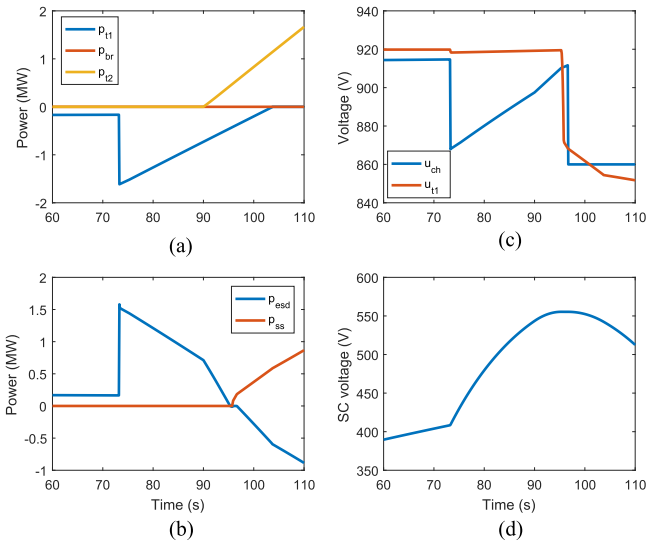

Fig. 13. Simulation results of the brake voltage following control with a long range.

high braking power, u_{t1} exceeds u_{br}, and the braking resistor is activated; in Fig. 12(b), the remaining energy is charged to the ESD; and in Fig. 12(d), u_{sc} rises to 459 V.

In contrast, the result with the proposed strategy is shown in Fig. 13. u_{t1} can be maintained at u_{br}. At the same time, the p_{br} has been fixed at 0, so that all energy is stored by the ESD. The maximum voltage of the SC is charged to 555 V to realize the maximum usage of ESD and inhibits the initiation of the brake resistor.

V. Main Track Experimental Validation

In order to prove the correctness of the proposed control strategy, a 1-MW SC-ESS is used, and the field test is divided into the Double Trains Experiment and Normal Operation Experiment on the Beijing Subway Batong Line. The experiment

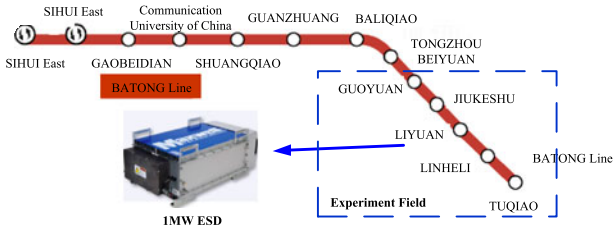

Fig. 14. Experiment field in the Beijing Subway Batong Line.

Fig. 15. Photos of the 1-MW ESD installed in LIYUAN substation.

TABLE III
Parameters of Batong Line Train

parameters	value	parameters	value
train formation	3M3T	maximum acceleration	1 m/s^2
overload condition	312.9 t	maximum deceleration	1 m/s^2
motor rated power	180 kW	maximum limit speed	80 km/h
inverter efficiency	0.93	motor efficiency	0.915
load power factor	0.85	gear efficiency	0.975

field is shown in the dashed frame of Fig. 14 with the average distance between two stations of around 1807.4 m, and ESD is installed in LIYUAN substation, in which the ESS is composed of a number of cabinets, as shown in Fig. 15. Train parameters are shown in Table III. The train is a B-type vehicle with 160 KVA of auxiliary capacity, and the rated voltage of dc traction power supply network is 750 V.

The SC cabinet is equipped with the 48 V/165 F SC module produced by Maxwell. The modules are connected with 2.7 V/3000 F monomers in 14 series and 10 parallels. The maximum storage energy is 7.4 kWh and can reach 1.34 MW under the rated voltage. The total capacity of ESD is 117.8 F with 8.82 mΩ of internal resistance. The rated voltage and current of ESD are 672 V and 2000 A, respectively.

A. Double Trains Experiment

In order to not affect the normal operation, the experiment with double trains is first carried on at night. There is respectively one train in the uplink and downlink lines.

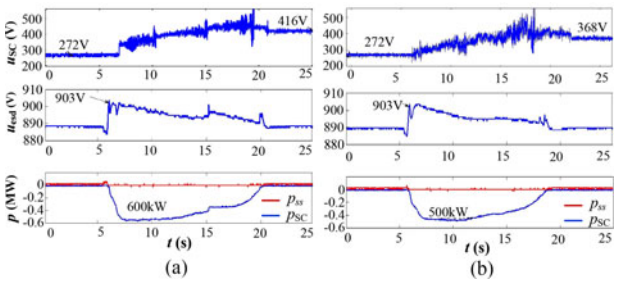

Fig. 16. Schematic diagram of double trains experiment. (a) Under proposed control strategy. (b) Under fixed charge threshold voltage of $u_{\text{ch}} = 900$ V.

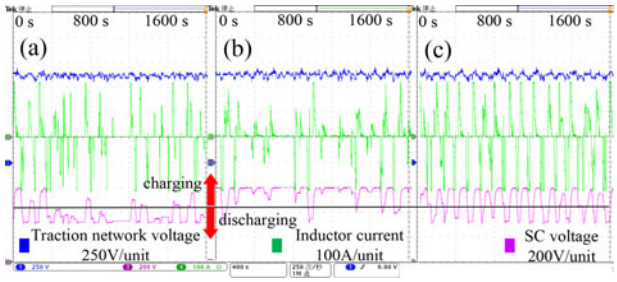

Fig. 17. Normal operation experiment waveforms of the ESD between 1–2000 s. (a) Worse charging condition with high u_{ch}. (b) Worse discharging condition with low u_{dis}. (c) A good waveform diagram under the proposed control strategy.

TABLE IV
ENERGY CONSUMPTION STATISTICS OF DOUBLE TRAIN EXPERIMENT

groups	$E_{\text{sc\_dis}}$ (kWh)	$E_{\text{sc\_ch}}$ (kWh)	E_{sub} (kWh)	E_{tra} (kWh)	η (%)
1	1.73	4.5	22.1	23.83	7.30
2	3.98	4.44	29.31	33.29	12
3	4	3.45	12.67	16.67	24.00
4	4.32	3.89	16.67	20.99	21
5	3.6	4.55	13.85	17.45	20.60
6	4.14	3.88	15.07	19.21	21.60

TABLE V
ENERGY SAVING STATISTICS OF A NORMAL OPERATION TEST

groups	$E_{\text{sc\_dis}}$ (kWh)	E_{sub} (kWh)	η (%)
1	1095.44	8480.37	12.9%
2	1062.25	7538.55	14.1%
3	1016.2	8213.36	12.4%
4	1096.6	7582.07	14.5%
5	1045.19	8307.33	12.6%
6	1101.84	8053.54	13.7%
7	1275.02	8791.2	14.5%

The train ran under the same conditions for the same interval. The first two groups in the experiment used the original fixed threshold control strategy, while the proposed control strategy was tested in the latter four groups. The special train interval and a braking situation are deliberately chosen for comparative analysis which are shown in Fig. 16. It can be seen that most of the remaining braking energy is stored in ESD. The $E_{\text{sc\_ch}}$ is 1.83 kWh in Fig. 16(a), while the energy is 1.51 kWh under the fixed threshold voltage of 900 V in Fig. 16(b). With the proposed control strategy, the SC will be charged to 416 V, and the single charging energy will be increased by 21.12%. Comparing with the fixed threshold condition, the reused braking energy is less, and it still can see the obvious energy saving effect from the power waveforms.

In the different experiment groups, the values are respectively counted in Table IV, η is defined as the ratio of $E_{\text{sc\_dis}}$ to E_{sub}.

Under different operating conditions, the charging and discharging thresholds of the ESD are controlled with the proposed control strategy. The SC ESS plays a major role in the energy saving process, with an average energy conservation rate of 21.7%.

B. Normal Operation Experiment

During the daytime normal operation experiment, the ESD is put into operation throughout the entire day. The waveforms of the ESD between 1–2000 s are shown in Fig. 17. Among them, Fig. 17(a) and (b) uses the fixed threshold control strategy, and Fig. 17(c) uses the proposed control strategy. From the above, the traction network voltage, the inductor current, and the SC voltage are shown in turn, where the inductor current is the single bridge arm inductor current of converter connected between the ESS and substation. Actually, the 1-MW ESS is made with the same two devices with one converter cabinet and one SC cabinet, which is good for the installation and control, and each converter contains four bridge arms. Thus, the current of the 1-MW ESS is eight times that of the single bridge arm inductor current. As it is shown, the ESS voltage curve of the red line directly reflects the stored maximum and minimum energy range of SC, and the middle black straight line points to every switch point in the process of charging and discharging.

u_{sc} range is 300–600 V. In Fig. 17(a), u_{oc} is 862 V, charging voltage u_{ch} is 894 V, and discharging voltage u_{dis} is 860 V. Due to the fact that the u_{ch} is excessively high, the energy is always consumed by the braking resistor, while the average u_{sc} is 384.5 V, and the $E_{\text{sc\_ch}}$ is only 65.1 kWh, with a poor energy recovery effect. In Fig. 17(b), u_{oc} rises up to 871 V, while the differential voltage of u_{dis} and u_{oc} increases, thus the ESD discharge power ratio decreases, resulting in the SC operating at a high voltage level. At the same time, due to the high SOC of the SC in the train braking process, it also cannot be effectively filled into; thus, the $E_{\text{sc\_ch}}$ is only 58.5 kWh, and the SC average voltage is 554.7 V. In Fig. 17(c), the issue of energy management strategy in Fig. 17(a) and (b) can be resolved, as the ESD can effectively absorb or release the regenerative braking energy. The average u_{sc} is 469.6 V, while $E_{\text{sc\_ch}}$ is 129.0 kWh; thus, the $E_{\text{sc\_ch}}$ is much greater and about twice as large as the energy in both Fig. 17(a) and (b). It also can be seen from Fig. 17(c) that the SC charges and discharges in a stable manner. Under the proposed control strategy, the charging and discharging cycle waveforms are evenly distributed up and down the horizontal straight line, which means that the capacity of the ESD can be fully utilized to achieve a good charging and discharging control. In addition, energy management state machine can operate in a very ideal state, which reflects the effectiveness and stability of the proposed energy management strategy.

After a period of normal operation, the statistic energy results are given in Table V. During this period of time, at least 1016 kWh can be saved per day, and the average η is 13.5%. It can be seen that the application of SC-ESD may help in achieving a significant energy-saving effect.

VI. Conclusion

In this paper, the energy distribution of urban rail transit was analyzed by means of a dc traction power system model, which includes the substation, train, brake resistor, and ESS. By performing a mathematical analysis of various states, the influence factors of energy distribution were studied, and the energy management strategy considering different conditions was proposed. By adjusting the charging and discharging thresholds, the maximum usage of energy storage devices was realized. Meanwhile, the proposed state switching system was able to achieve smooth alteration between different management statuses. Based on the actual operation data of the Beijing Batong Subway Line, a simulation and field experiments were carried out. In the case studies, by using the proposed energy management strategy, the average energy conservation in the night double trains experiment reached as high as 21.7%. In the normal operation experiment, the daily energy saving was at least 1016 kWh, while the average energy conservation was 13.5%. It is thus proven that the energy management strategy of this paper can make full use of the SC ESS, and thereby achieve a significant energy-saving effect.

References

[1] A. González-Gil, R. Palacin, P. Batty, and J. P. Powell, "A systems approach to reduce urban rail energy consumption," *Energy Convers. Manage.*, vol. 80, pp. 509–524, 2014, doi 10.1016/j.enconman.2014.01.060.

[2] M. Andriollo, R. Benato, M. Bressan, S. Sessa, F. Palone, and R. Polito, "Review of power conversion and conditioning systems for stationary electrochemical storage," *Energies*, vol. 8, no. 2, pp. 960–975, 2015, doi 10.3390/en8020960.

[3] K. Divya and J. Stergaard, "Battery energy storage technology for power systems an overview," *Electr. Power Syst. Res.*, vol. 79, no. 4, pp. 511–520, 2009.

[4] I. Hadjipaschalis, A. Poullikkas, and V. Efthimiou, "Overview of current and future energy storage technologies for electric power applications," *Renew. Sustain. Energy Rev.*, vol. 13, nos. 6/7, pp. 1513–1522, 2009, doi 10.1016/j.rser.2008.09.028.

[5] A.-L. Allegre, A. Bouscayrol, P. Delarue, P. Barrade, E. Chattot, and S. El-Fassi, "Energy storage system with supercapacitor for an innovative subway," *IEEE Trans. Ind. Electron.*, vol. 57, no. 12, pp. 4001–4012, Dec. 2010, doi 10.1109/tie.2010.2044124.

[6] P. J. Grbovic, P. Delarue, P. Le Moigne, and P. Bartholomeus, "A bidirectional three-level dc–dc converter for the ultracapacitor applications," *IEEE Trans. Ind. Electron.*, vol. 57, no. 10, pp. 3415–3430, Oct. 2010, doi 10.1109/tie.2009.2038338.

[7] M. Carpita, M. De Vivo, and S. Gavin, "Dynamic modeling of a bidirectional dc/dc interleaved converter working in discontinuous mode for stationary and traction supercapacitor applications," in *Proc. Int. Symp. Power Electron. Power Electron., Electr. Drives, Autom. Motion*, 2012, pp. 1306–1313.

[8] S. M. Kim and S. K. Sul, "Control of rubber tyred gantry crane with energy storage based on supercapacitor bank," *IEEE Trans. Power Electron.*, vol. 21, no. 5, pp. 1420–1427, Sep. 2006, doi 10.1109/tpel.2006.880260.

[9] M. B. Camara, H. Gualous, F. Gustin, and A. Berthon, "Design and new control of dc/dc converters to share energy between supercapacitors and batteries in hybrid vehicles," *IEEE Trans. Veh. Technol.*, vol. 57, no. 5, pp. 2721–2735, Sep. 2008, doi 10.1109/tvt.2008.915491.

[10] A. J. Lopez-Lopez, R. R. Pecharroman, A. Fernandez-Cardador, and A. P. Cucala, "Assessment of energy-saving techniques in direct-current-electrified mass transit systems," *Transp. Res. Part C: Emerg. Technol.*, vol. 38, pp. 85–100, 2014, doi 10.1016/j.trc.2013.10.011.

[11] R. Barrero, X. Tackoen, and J. Van Mierlo, "Stationary or onboard energy storage systems for energy consumption reduction in a metro network," *Proc. Inst. Mech. Eng., Part F: J. Rail Rapid Transit*, vol. 224, no. 3, pp. 207–225, 2010.

[12] L. Battistelli, M. Fantauzzi, D. Iannuzzi, and D. Lauria, "Energy management of electrified mass transit systems with energy storage devices," in *Proc. Int. Symp. Power Electron., Electr. Drives, Autom. Motion*, 2012, pp. 1172–1177.

[13] P. J. Grbovic, P. Delarue, P. Le Moigne, and P. Bartholomeus, "Modeling and control of the ultracapacitor-based regenerative controlled electric drives," *IEEE Trans. Ind. Electron.*, vol. 58, no. 8, pp. 3471–3484, Aug. 2011.

[14] F. Ciccarelli, D. Iannuzzi, and P. Tricoli, "Speed-based supercapacitor state of charge tracker for light railway vehicles," in *Proc. 14th Eur. Conf. Power Electron. Appl.*, 2011, pp. 1–12.

[15] F. Ciccarelli, A. Del Pizzo, and D. Iannuzzi, "Improvement of energy efficiency in light railway vehicles based on power management control of wayside lithium-ion capacitor storage," *IEEE Trans. Power Electron.*, vol. 29, no. 1, pp. 275–286, Jan. 2014.

[16] M. Miyatake and K. Matsuda, "Optimal speed and charge/discharge control of a train with onboard energy storage devices for minimum energy operation," in *Proc. Int. Symp. Power Electron., Electr. Drives, Autom. Motion*, 2008, pp. 1211–1216.

[17] A. Rufer, D. Hotellier, and P. Barrade, "A supercapacitor-based energy storage substation for voltage compensation in weak transportation networks," *IEEE Trans. Power Del.*, vol. 19, no. 2, pp. 629–636, Apr. 2004.

[18] F. Ciccarelli, D. Iannuzzi, and P. Tricoli, "Control of metro-trains equipped with onboard supercapacitors for energy saving and reduction of power peak demand," *Transp. Res. Part C: Emerg. Technol.*, vol. 24, pp. 36–49, 2012, doi 10.1016/j.trc.2012.02.001.

[19] D. Iannuzzi, E. Pagano, and P. Tricoli, "The use of energy storage systems for supporting the voltage needs of urban and suburban railway contact lines," *Energies*, vol. 6, no. 4, pp. 1802–1820, 2013.

[20] F. Ciccarelli, D. Iannuzzi, K. Kondo, and L. Fratelli, "Line-voltage control based on wayside energy storage systems for tramway networks," *IEEE Trans. Power Electron.*, vol. 31, no. 1, pp. 884–899, Jan. 2016, doi 10.1109/tpel.2015.2411996.

[21] P. J. Grbovic, P. Delarue, P. Le Moigne, and P. Bartholomeus, "The ultracapacitor-based regenerative controlled electric drives with power-smoothing capability," *IEEE Trans. Ind. Electron.*, vol. 59, no. 12, pp. 4511–4522, Dec. 2012.

[22] H. Lee, E. Joung, G. Kim, and C. An, "A study on the effects of energy storage system," in *Proc. Int. Conf. Inf. Multimedia Technol.*, 2009, pp. 28–32.

[23] R. Teymourfar *et al.*, "Stationary super-capacitor energy storage system to save regenerative braking energy in a metro line," *Energy Convers. Manage.*, vol. 56, pp. 206–214, 2012.

[24] A. González-Gil, R. Palacin, and P. Batty, "Sustainable urban rail systems: Strategies and technologies for optimal management of regenerative braking energy," *Energy Convers. Manag.*, vol. 75, pp. 374–388, 2013.

[25] R. Teymourfar, G. Farivar, H. Iman-Eini, and B. Asaei, "Optimal stationary super-capacitor energy storage system in a metro line," in *Proc. 2nd Int. Conf. Electr. Power Energy Convers. Syst.*, 2011, pp. 1–5.

[26] B. Wang, Z. Yang, F. Lin, and W. Zhao, "An improved genetic algorithm for optimal stationary energy storage system locating and sizing," *Energies*, vol. 7, no. 10, pp. 6434–6458, 2014.

[27] D. Pavković, M. Hoić, J. Deur, and J. Petrić, "Energy storage systems sizing study for a high-altitude wind energy application," *Energy*, vol. 76, pp. 91–103, 2014.

Zhihong Yang (S'16) received the B.S. degree in electrical engineering, in 2015 from Beijing Jiaotong University, Beijing, China, where she is currently working toward the Master's degree with the School of Electrical Engineering.

Her research interests include energy management strategies of energy storage systems, energy-efficient models, and optimal operation of multiple trains in urban rail transit.

Zhongping Yang (M'14) received the B.Eng. degree from Tokyo University of Mercantile Marine, Tokyo, Japan, in 1997 and the M.Eng. and Ph.D. degrees from the University of Tokyo, Tokyo, Japan, in 1999 and 2002, respectively, all in electrical engineering.

He is currently a Professor with the School of Electrical Engineering, Beijing Jiaotong University, Beijing, China. His research interests include high-speed rail integration technology, traction and regenerative braking technology, and wireless power transfer of urban rail vehicles.

Prof. Yang received the Zhan Tianyou Award for Science and Technology in 2010, the Excellent Popular Science and Technology Book Award in 2011, and the Science and Technology Progress Award (second prize) of Ministry of Education in China in 2016.

Huan Xia (S'14–M'17) received the B.S. degree in electrical engineering from Hefei University of Technology, Hefei, China, in 2009 and the Ph.D. degree in vehicle operation engineering from Beijing Jiaotong University, Beijing, China, in 2017.

He is currently with Beijing Institute of Space Launch Technology. His research interests include dc/dc converters, energy storage systems, and hybrid power systems.

Fei Lin (M'05) received the B.S. degree from Xi'an Jiaotong University, Xi'an, China; the M.S. degree from Shandong University, Jinan, China; and the Ph.D. degree from Tsinghua University, Beijing, China, in 1997, 2000, and 2004, respectively, all in electrical engineering.

He is currently a Professor with the School of Electrical Engineering, Beijing Jiaotong University. His research interests include traction converters and motor drives, energy management for railway systems, and digital control of power-electronic-based devices.